bioRxiv preprint doi: https://doi.org/10.1101/2024.08.26.609742; this version posted August 27, 2024. The copyright holder for this preprint (which was not certified by peer review) is the author/funder, who has granted bioRxiv a license to display the preprint in perpetuity. It is made available under aCC-BY-NC-ND 4.0 International license.

Fig.S1 Overview of animal models. A: Workflow of generation of *epsin1* $^{fl/fl}$, *epsin2* $^{-/-}$, Albumin Cre $^{+/-}$ (Liver-DKO), *epsin1* $^{+/+}$, and *epsin2* $^{+/+}$, Albumin Cre $^{+/-}$ as control group (WT). B: Workflow of generation of *epsin1* $^{fl/fl}$, *epsin2* $^{-/-}$, Albumin Cre $^{+/-}$, *Apoe* $^{-/-}$ (Liver-DKO / *Apoe* $^{-/-}$), and *epsin1* $^{+/+}$, *epsin2* $^{+/+}$, Albumin Cre $^{+/-}$, *Apoe* $^{-/-}$ as control group (WT / *Apoe* $^{-/-}$).

Fig.S2 Elevated epsin1 and epsin2 expression in the aorta from CAD patients, and recruitment of CD68 positive macrophages in the aorta from CAD patients that colocalization to both epsin1 and epsin2. A: Immunofluorescence co-stain of epsin1 and CD68 antibodies in aortas from both healthy control and CAD patients, epsin1 is in red color, CD68 is in green color, and DAPI is used for nuclei stain. The atherosclerotic lesion is encircled with dashed line in CAD patients. B: Immunofluorescence co-stain of epsin2 and CD68 antibodies in aortas from both healthy control and CAD patients, epsin2 is in red color, CD68 is in green color, and DAPI is used for nuclei stain. The atherosclerotic lesion is highlighted that below the dashed line in CAD patients. C: Quantification of epsin1 and epsin2 immunofluorescence signal intensity between healthy control and CAD patients. CD68 expression is highly colocalized with both epsin1 and epsin2 in CAD patients, and the overlay percentage between CD68 and epsin1 or CD68 and epsin2 are quantified. N=5, *** $p<0.001$.

Fig.S3 Elevated expression of epsin1 and epsin2 but diminished expression of LDLR protein in hepatocytes from the livers of NASH patients. A: Immunofluorescence staining of epsin1, epsin2 , LDLR and albumin protein in the livers of healthy control (left) and NASH patients (right). LDLR protein signals in green color, and albumin protein signals in red color, DAPI is used for nuclei stain. B: Quantification of epsin1, epsin2, LDLR immunofluorescence signal intensity in both healthy control and NASH patients. N=5, *** $p<0.001$.

bioRxiv preprint doi: https://doi.org/10.1101/2024.08.26.609742; this version posted August 27, 2024. The copyright holder for this preprint (which was not certified by peer review) is the author/funder, who has granted bioRxiv a license to display the preprint in perpetuity. It is made available under aCC-BY-NC-ND 4.0 International license.

Fig.S4 Diminished HNF4α expression level in NASH (Cirrhosis) patients. A: Immunofluorescence stain of HNF4α in the liver from both healthy control and cirrhosis patients (left), HNF4α is in green color, and DAPI is used for nuclei stain. Quantification of HNF4α immunofluorescence signal intensity between healthy control and cirrhosis patients (right). B: Western blot of HNF4α for the liver lysates from biopsy in both healthy control and NASH patients, beta-Actin is used as internal reference (left), the quantification of HNF4α expression in both healthy control and cirrhosis patients (right). C: Relative expression of HNF4α mRNA in both healthy control and NASH patients measured by RT-qPCR. N=3, * $p<0.05$, ** $p<0.01$, *** $p<0.001$.

Fig. S5: Single-cell RNA-sequencing reveals hepatocyte transition in Liver-DKO mice on an ApoE$^{-/-}$ background. A: A relatively high proportion of HC Hnf4α^{hi} in ApoE$^{-/-}$/Liver-DKO and a relatively high proportion of HC2 Alb^{hi} and HC3 Alb^{hi} of ApoE$^{-/-}$. B: Pseudotime trajectory and Rna velocity analysis mapping the transition pathway from lipogenic Alb^{hi} hepatocytes to glucogenic Hnf4α^{hi} hepatocytes in ApoE$^{-/-}$/Liver-DKO, in contrast to ApoE$^{-/-}$. C-E: CellRank analysis indicating more dynamic shifts from lipogenic Alb^{hi} hepatocytes to glucogenic Hnf4α^{hi} hepatocytes in ApoE$^{-/-}$/Liver-DKO compared to ApoE$^{-/-}$. CellRank probability calculation for hepatocyte sub-cell populations in ApoE$^{-/-}$ (C), and in ApoE$^{-/-}$/Liver-DKO (E). D-F: Violin plots show transition probabilities of initial to terminal states within hepatocyte sub-cell populations. in ApoE$^{-/-}$ controls (D), and in ApoE$^{-/-}$/Liver-DKO mice (F). **Note:** We used the two-sample proportion test to compare the cell's proportion in panel (A).

Fig.S6: Comprehensive cell type-specific gene markers and their corresponding expressions. A: UMAP visualization of ApoE$^{-/-}$/Liver-DKO cell populations compared to ApoE$^{-/-}$. B: Dot plot illustrating the percentage of cells expressing each gene marker corresponding to specific cell types in ApoE$^{-/-}$/Liver-DKO and ApoE$^{-/-}$ mice. The size of the dots represents the proportion of cells expressing the marker, while the color intensity indicates the expression level of the gene marker in each cell type.

Fig.S7: Diminished expression of lipogenic genes and elevated apolipoprotein genes are identified as indicators of inhibition of lipogenesis in HNF4α^{hi} hepatocytes. A: Feature plots show diminished expression of lipogenic genes in ApoE$^{-/-}$/Liver-DKO compared to ApoE$^{-/-}$. B: Shows gene expression dynamic with respect to pseudo time from Alb^{hi} to Hnf4 α^{hi} hepatocytes. The elevated HNF4α expression in HNF4α^{hi} hepatocytes is positively correlated to the diminished expression of Acaca and the elevated expression of Apoa4 and Apob in ApoE$^{-/-}$/Liver-DKO.

Fig.S8: Enhanced GO pathways enriched in plasma lipoprotein particle clearance and diminished glycolytic process in ApoE$^{-/-}$/Liver-DKO hepatocytes. A-C: CNET plots highlight the specific GO pathway enrichments related to genes upregulated in ApoE$^{-/-}$/Liver-DKO within the hepatocyte subtypes. D-G: CNET plots highlight the GO pathway enrichments related to genes downregulated in ApoE$^{-/-}$/Liver-DKO within the hepatocyte sub-populations. **Note:** The edge color represents different pathways, and the corresponding circle's number indicates the number of genes associated with the pathway.

bioRxiv preprint doi: https://doi.org/10.1101/2024.08.26.609742; this version posted August 27, 2024. The copyright holder for this preprint (which was not certified by peer review) is the author/funder, who has granted bioRxiv a license to display the preprint in perpetuity. It is made available under aCC-BY-NC-ND 4.0 International license.

Fig.S9: Enhanced Rorα-cholesterol and Sdc4-Fn1 communication pathways and diminished Bsg-Ppia and Nr1h4-AndrosteroneHSD17B6 communication pathways in ApoE$^{-/-}$/Liver-DKO hepatocytes. A: Chord plot highlights the specific Rorα-cholesterol and Sdc4-Fn1 communication related to genes and metabolites upregulated in ApoE$^{-/-}$/Liver-DKO. B: Chord plot exhibits the specific Bsg-Ppia and Nr1h4-AndrosteroneHSD17B6 communication associated to genes and metabolites downregulated in ApoE$^{-/-}$/Liver-DKO. **Note:** Edge and outer lower half-circle colors represent sender cell types, while inner lower and upper half-circle colors indicate receiver cell types.

Fig.S10: Elevated gene expression related to glycogenesis and diminished lipogenic gene expression in ApoE$^{-/-}$/Liver-DKO as compared to ApoE$^{-/-}$, shown through single-cell analysis and real-time quantitative PCR (qPCR) validation. A: Violin plots of gene expression related to glycogenesis (Gys2, Gck, Pgm1) and lipogenesis (Acly) and cholesterol clearance (Apoa2, Apob) in ApoE$^{-/-}$/Liver-DKO as compared to ApoE$^{-/-}$, shown through single-cell analysis B: Validation of genes expression involved in glycogenesis and lipogenesis by real-time quantitative PCR (qPCR) in the liver from both ApoE$^{-/-}$ and ApoE$^{-/-}$/Liver-DKO mice. N=3, * $p<0.05$, ** $p<0.001$, *** $p<0.0001$.

Fig.S11: Elevated gene expression related to glycogenesis and diminished lipogenic gene expression in different clustered hepatocytes, including HC1 Alb^{hi}, HC2 Alb^{hi}, HC3 Alb^{hi}, and HC HNF4α^{hi} in ApoE$^{-/-}$/Liver-DKO as compared to ApoE$^{-/-}$. A: Downregulated expression of lipogenic genes, such as Scd1, Acaca, but with upregulated expression apolipoprotein genes (Apoa4, Apob) in different clustered hepatocytes in the liver of ApoE$^{-/-}$/Liver-DKO, indicates diminished lipogenesis and elevated capacity for low-density lipoprotein clearance in the liver of ApoE$^{-/-}$/Liver-DKO. B: Upregulated expression of glycogenic genes, such as Pgm1, Gys2, and Ugp2, in different clustered hepatocytes in the liver of ApoE$^{-/-}$/Liver-DKO, reveals elevated glycogenesis in the liver of ApoE$^{-/-}$/Liver-DKO.

Fig.S12: Diminished apolipoprotein genes expression in hPCSK9-D374Y mutant compared with control. Downregulated expression of apolipoprotein genes, such as Apoa1, Apoa2, Apoa4, Apoc1, Apoc2, Apoc3 and Apob, in different clustered hepatocytes (HC1, HC2, HC3) in hPCSK9-D374Y mutant compared with control, indicates diminished low-density lipoprotein clearance in hPCSK9-D374Y mutant.

Fig.S13: Diminished HNF4α and elevated epsin1 expression in the different clustered hepatocytes in the liver from hPCSK9-D374Y mutant. Downregulated expression of genes involved in the transportation of low-density lipoprotein cholesterol and lipogenesis, such as Ldlr, Abca1, and genes participate in fatty acid metabolism (Sdc4) in the different clustered hepatocytes in the liver from hPCSK9-D374Y mutant, indicates the dyslipidemia in hPCSK9-D374Y mutant. Diminished HNF4α and Albumin expression in the different clustered hepatocytes (HC1, HC2, HC3) in the liver in hPCSK9-D374Y mutant, which negatively correlated to its elevated epsin1 expression.

Fig.S14: Elevated expression lipogenic genes and diminished glycogenic genes in the different clustered hepatocytes in the liver in hPCSK9-D374Y mutant. A: Upregulated expression of

bioRxiv preprint doi: https://doi.org/10.1101/2024.08.26.609742; this version posted August 27, 2024. The copyright holder for this preprint (which was not certified by peer review) is the author/funder, who has granted bioRxiv a license to display the preprint in perpetuity. It is made available under aCC-BY-NC-ND 4.0 International license.

genes involved in lipogenesis, such as Acly and Fasn, in the different clustered hepatocytes in the liver in hPCSK9-D374Y mutant. B: Downregulated expression of genes that participate in glycogenesis, such as Gys2 and Ugp2, in the different clustered hepatocytes in the liver in hPCSK9-D374Y mutant.

bioRxiv preprint doi: https://doi.org/10.1101/2024.08.26.609742; this version posted August 27, 2024. The copyright holder for this preprint (which was not certified by peer review) is the author/funder, who has granted bioRxiv a license to display the preprint in perpetuity. It is made available under aCC-BY-NC-ND 4.0 International license.

Fig.S1

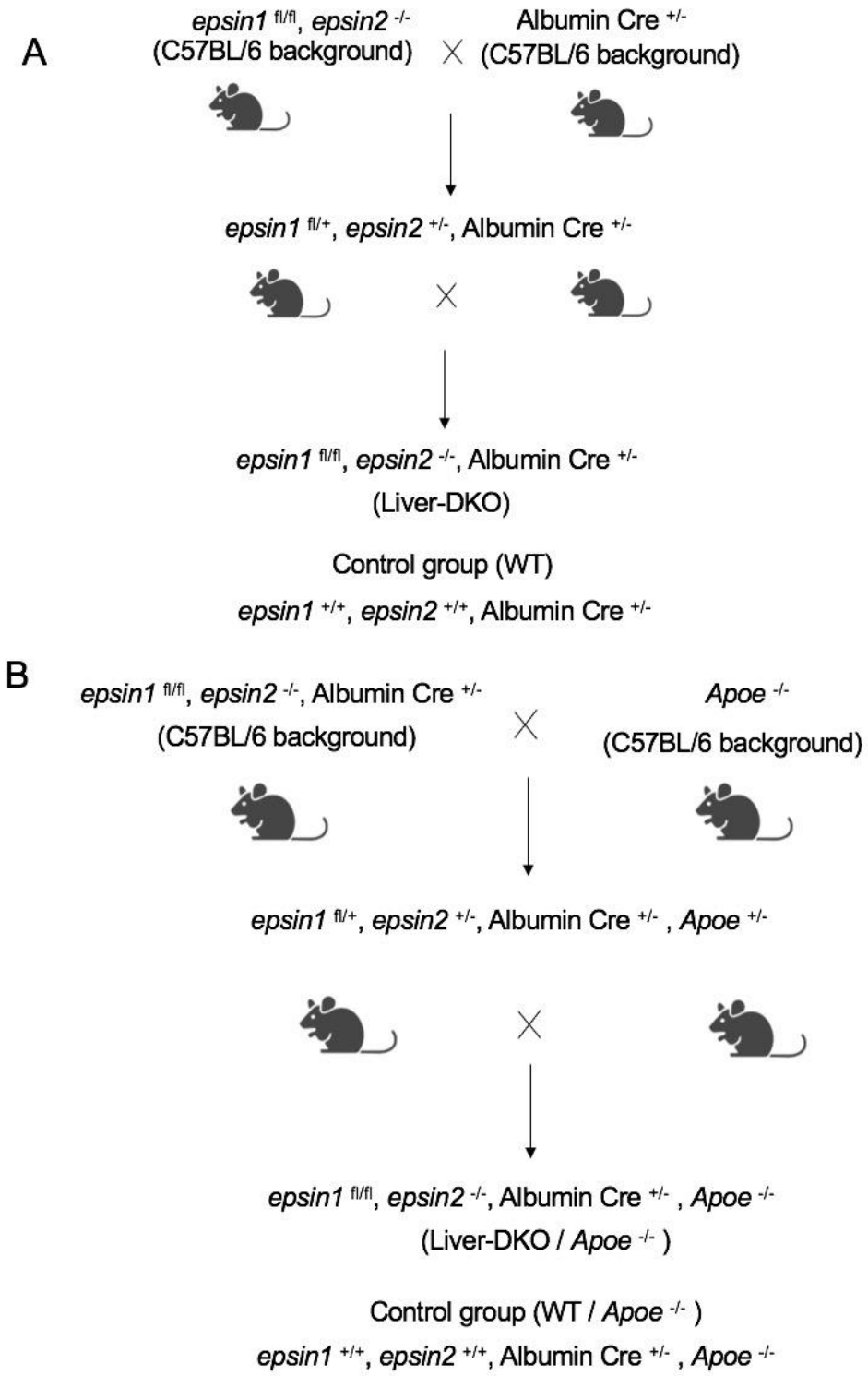

bioRxiv preprint doi: https://doi.org/10.1101/2024.08.26.609742; this version posted August 27, 2024. The copyright holder for this preprint (which was not certified by peer review) is the author/funder, who has granted bioRxiv a license to display the preprint in perpetuity. It is made available under aCC-BY-NC-ND 4.0 International license.

Fig.S2

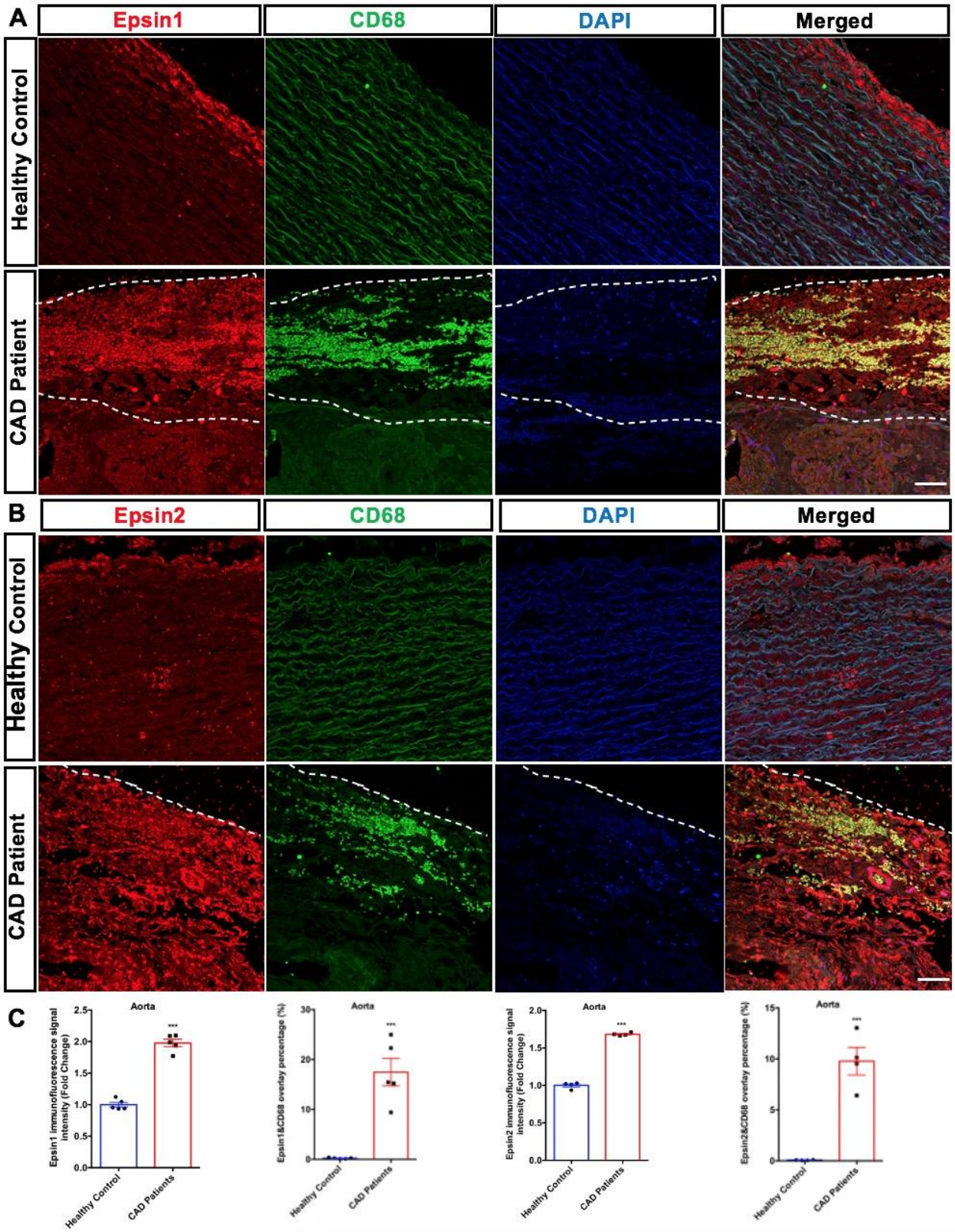

bioRxiv preprint doi: https://doi.org/10.1101/2024.08.26.609742; this version posted August 27, 2024. The copyright holder for this preprint (which was not certified by peer review) is the author/funder, who has granted bioRxiv a license to display the preprint in perpetuity. It is made available under aCC-BY-NC-ND 4.0 International license.

1630
1631
1632 **Fig.S3**

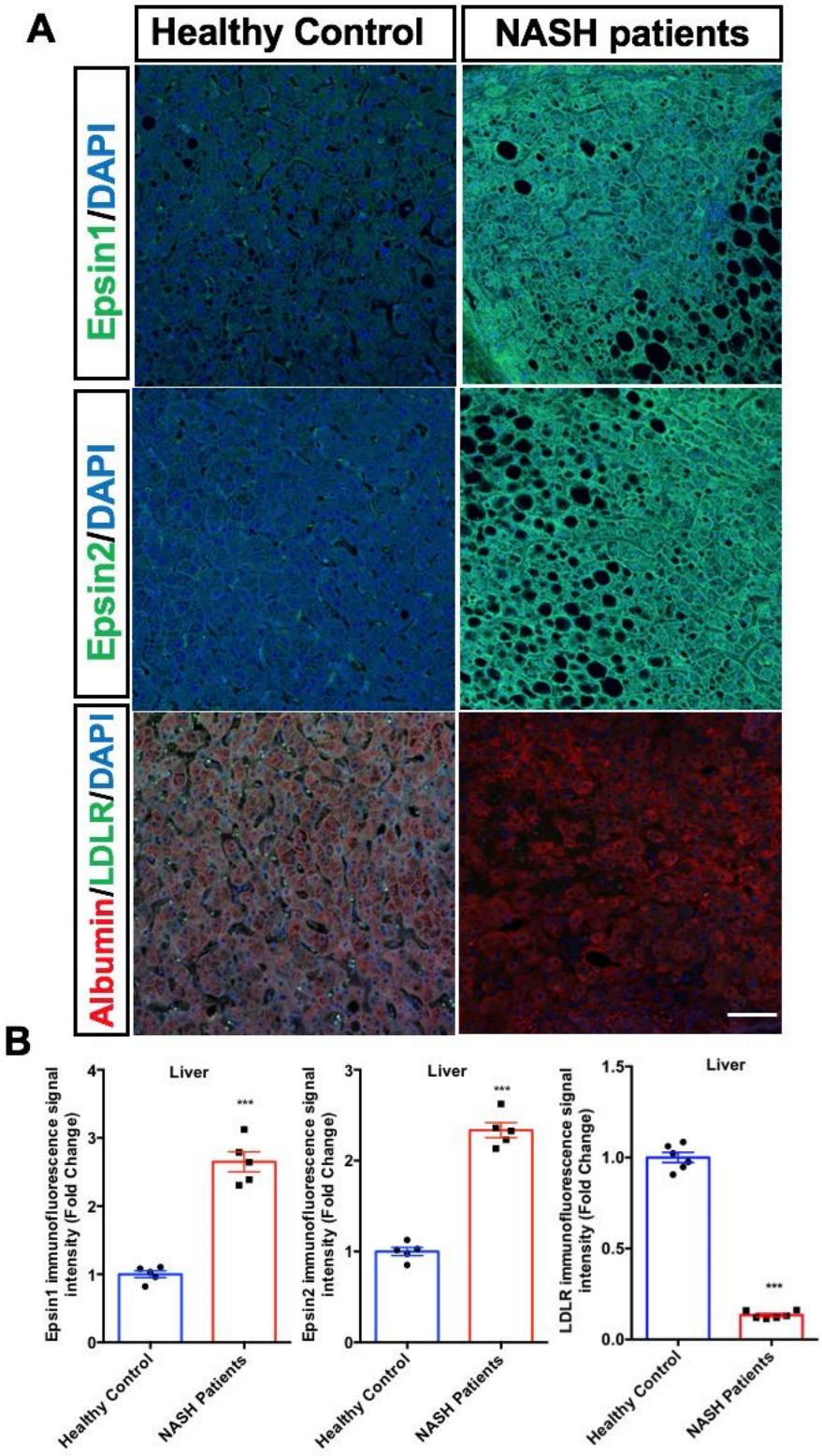

1633

bioRxiv preprint doi: https://doi.org/10.1101/2024.08.26.609742; this version posted August 27, 2024. The copyright holder for this preprint (which was not certified by peer review) is the author/funder, who has granted bioRxiv a license to display the preprint in perpetuity. It is made available under aCC-BY-NC-ND 4.0 International license.

Fig.S4

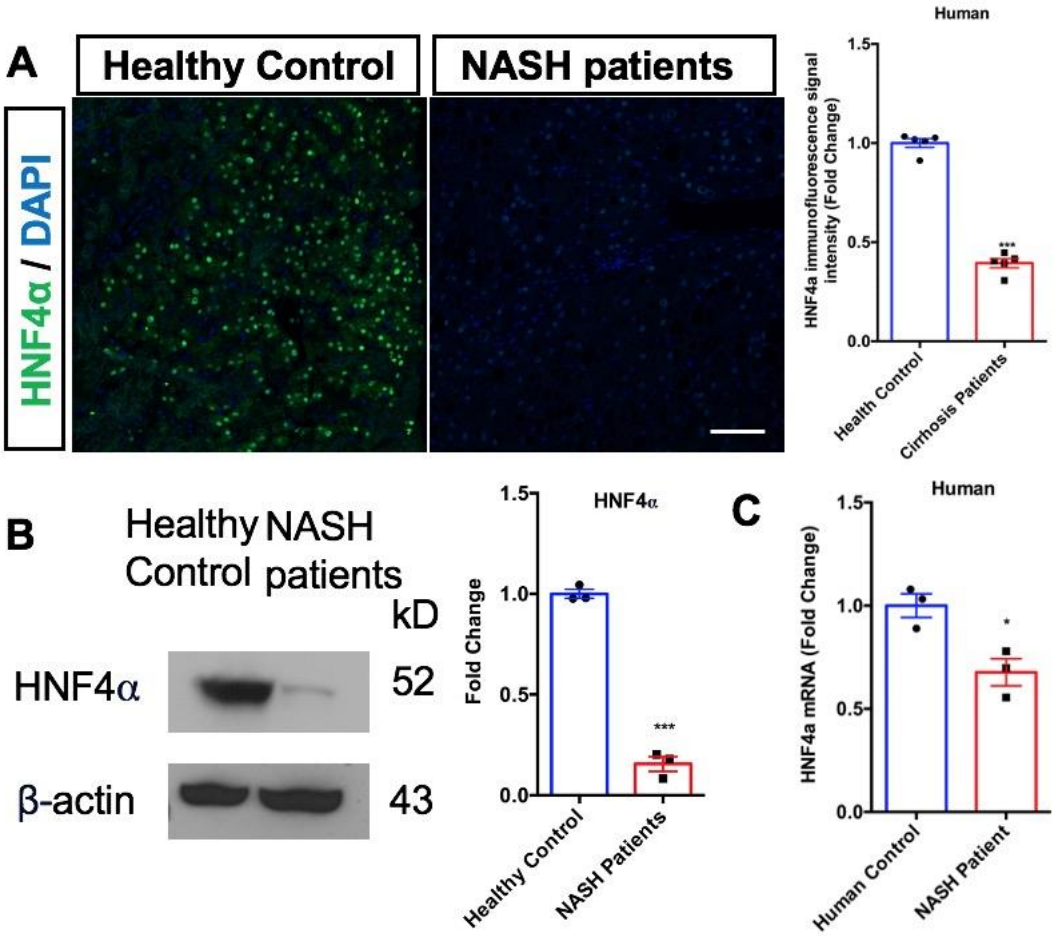

bioRxiv preprint doi: https://doi.org/10.1101/2024.08.26.609742; this version posted August 27, 2024. The copyright holder for this preprint (which was not certified by peer review) is the author/funder, who has granted bioRxiv a license to display the preprint in perpetuity. It is made available under aCC-BY-NC-ND 4.0 International license.

Fig.S5

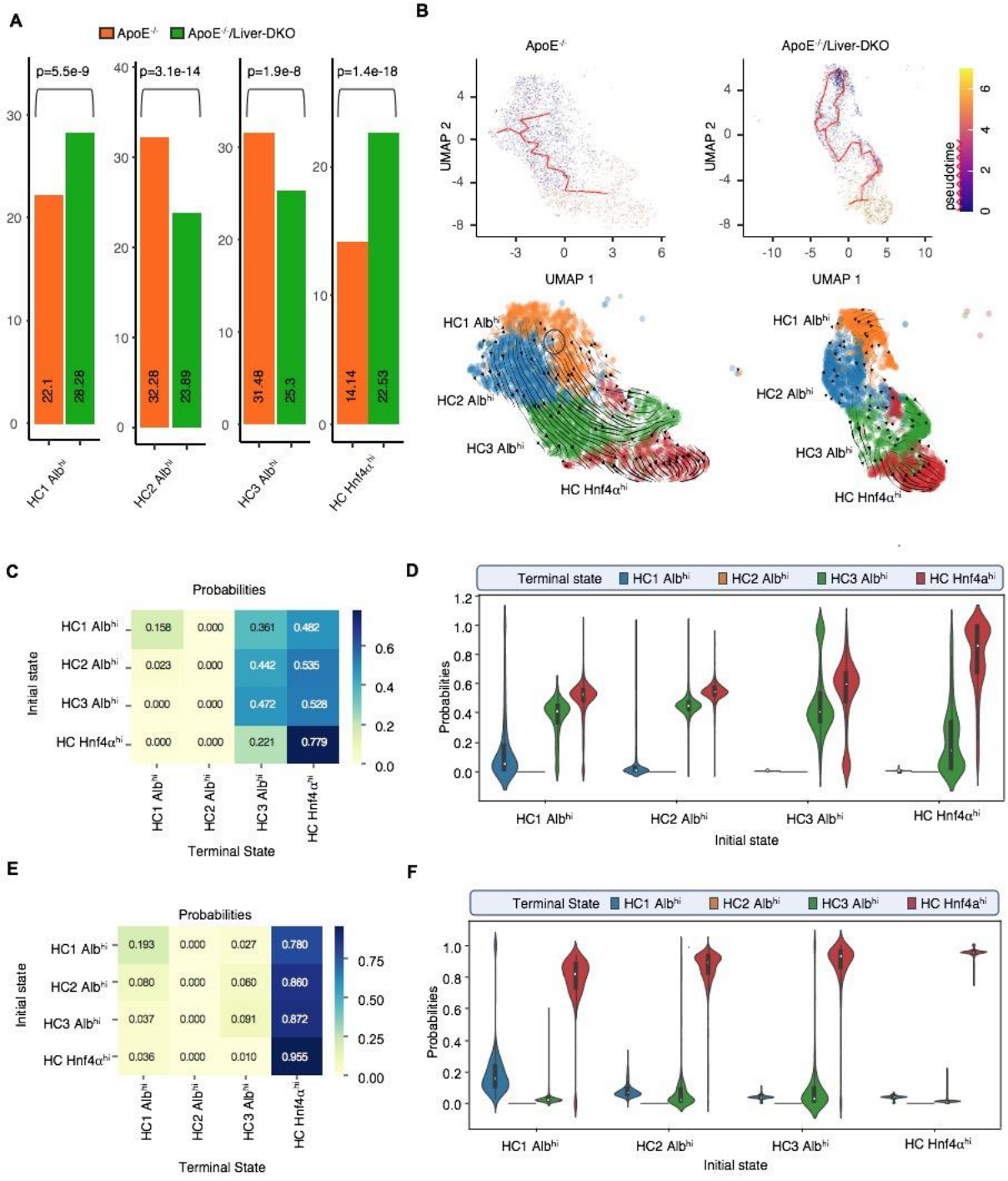

bioRxiv preprint doi: https://doi.org/10.1101/2024.08.26.609742; this version posted August 27, 2024. The copyright holder for this preprint (which was not certified by peer review) is the author/funder, who has granted bioRxiv a license to display the preprint in perpetuity. It is made available under aCC-BY-NC-ND 4.0 International license.

Fig.S6

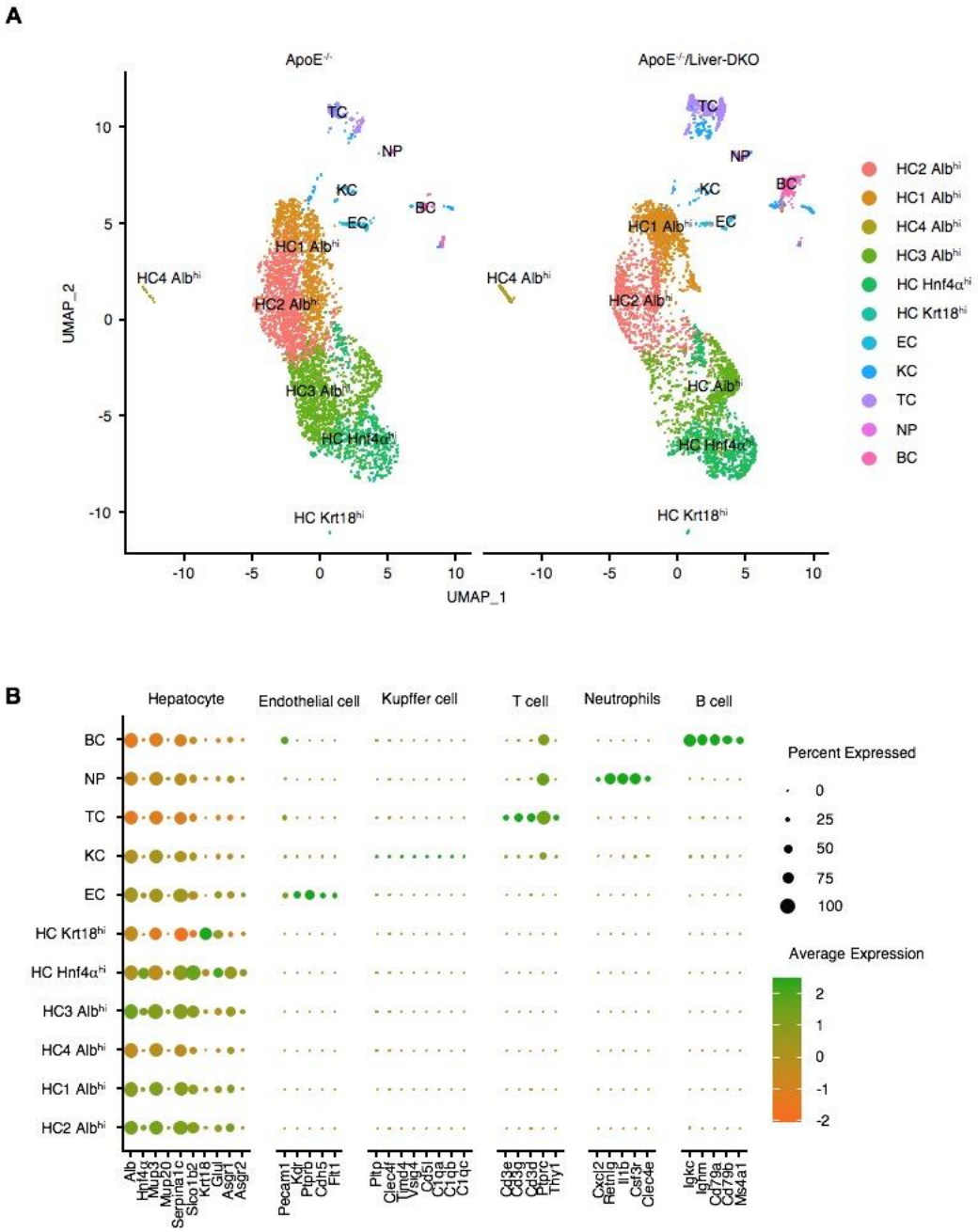

bioRxiv preprint doi: https://doi.org/10.1101/2024.08.26.609742; this version posted August 27, 2024. The copyright holder for this preprint (which was not certified by peer review) is the author/funder, who has granted bioRxiv a license to display the preprint in perpetuity. It is made available under aCC-BY-NC-ND 4.0 International license.

Fig.S7

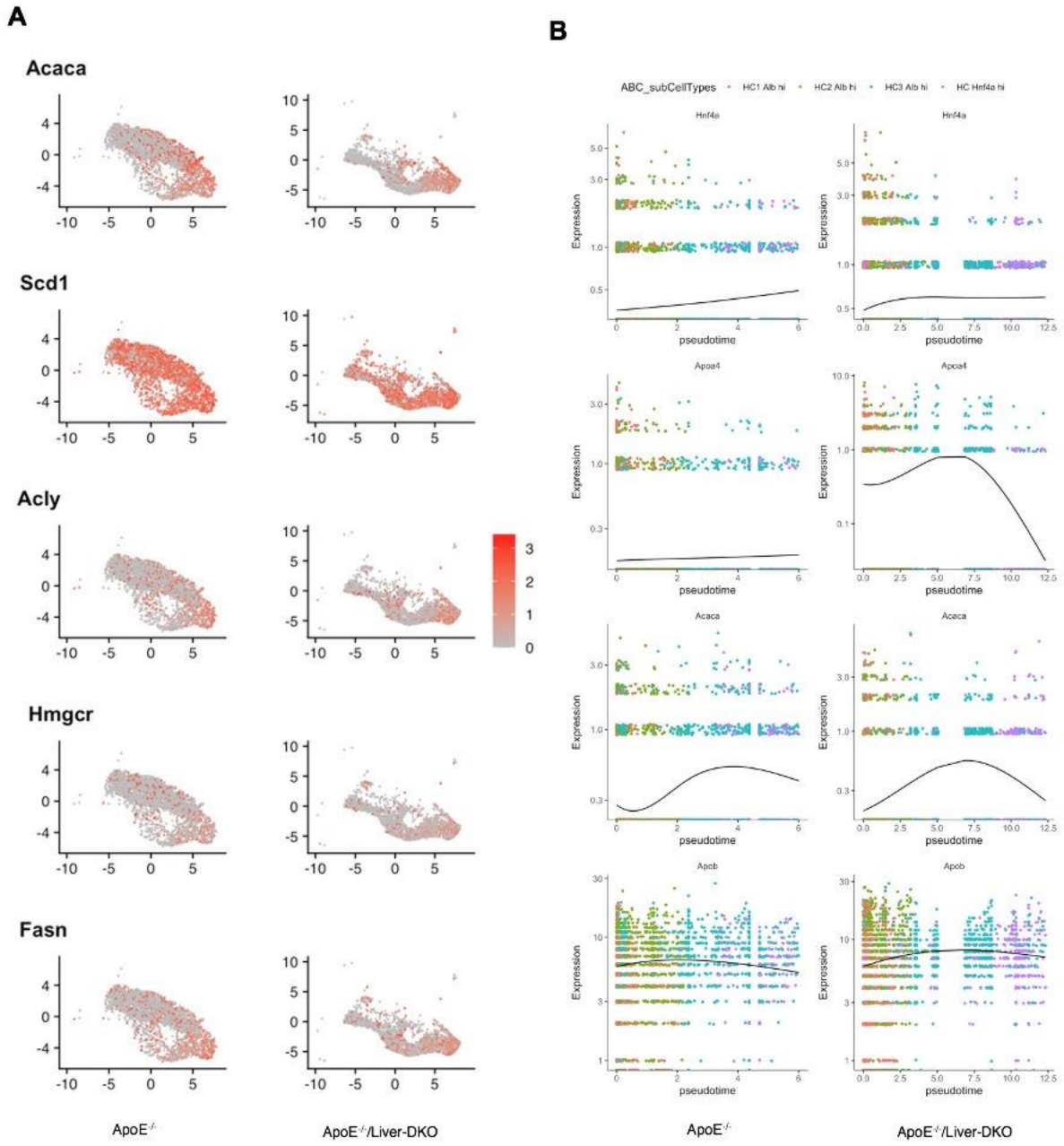

bioRxiv preprint doi: https://doi.org/10.1101/2024.08.26.609742; this version posted August 27, 2024. The copyright holder for this preprint (which was not certified by peer review) is the author/funder, who has granted bioRxiv a license to display the preprint in perpetuity. It is made available under aCC-BY-NC-ND 4.0 International license.

Fig.S8

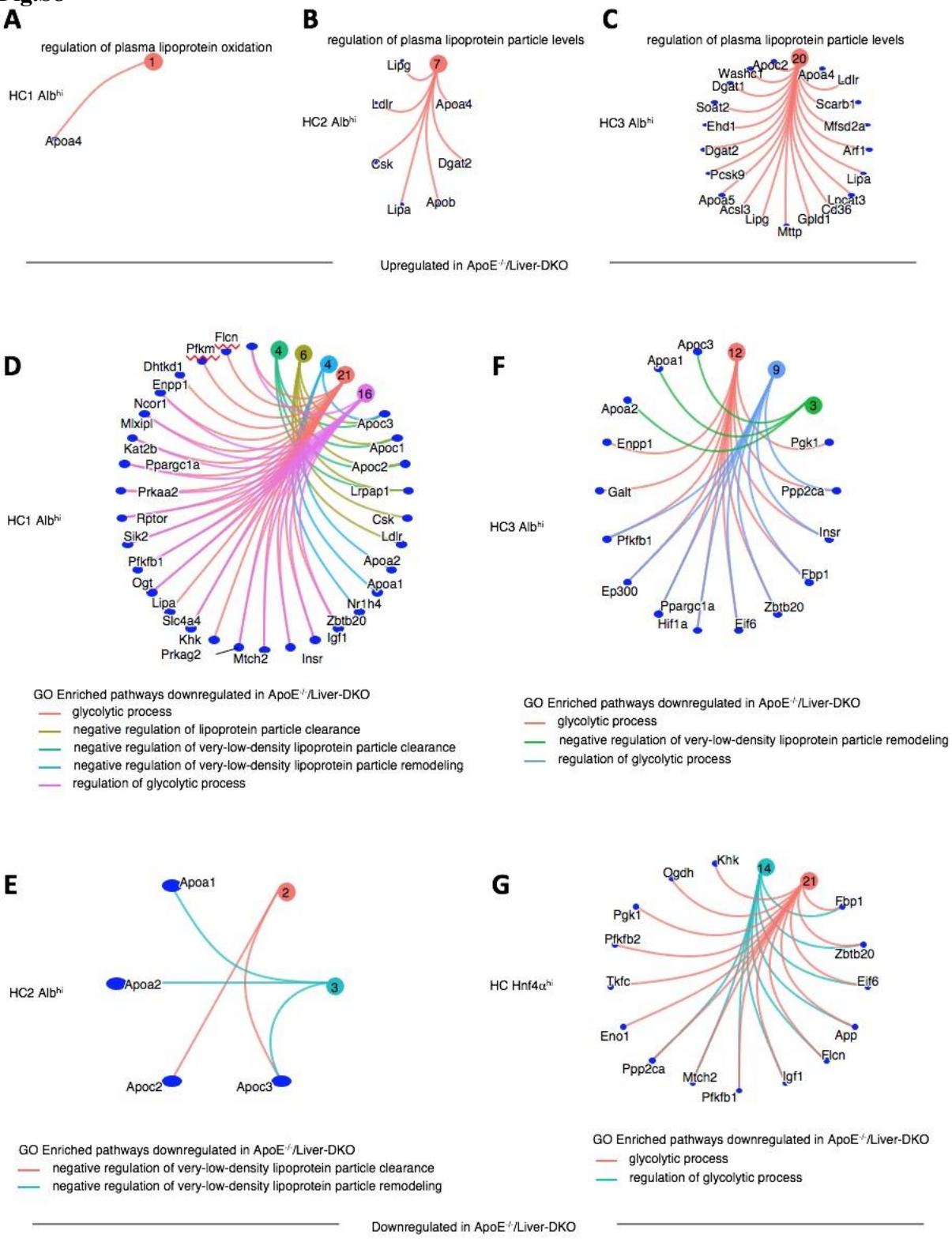

bioRxiv preprint doi: https://doi.org/10.1101/2024.08.26.609742; this version posted August 27, 2024. The copyright holder for this preprint (which was not certified by peer review) is the author/funder, who has granted bioRxiv a license to display the preprint in perpetuity. It is made available under aCC-BY-NC-ND 4.0 International license.

Fig.S9

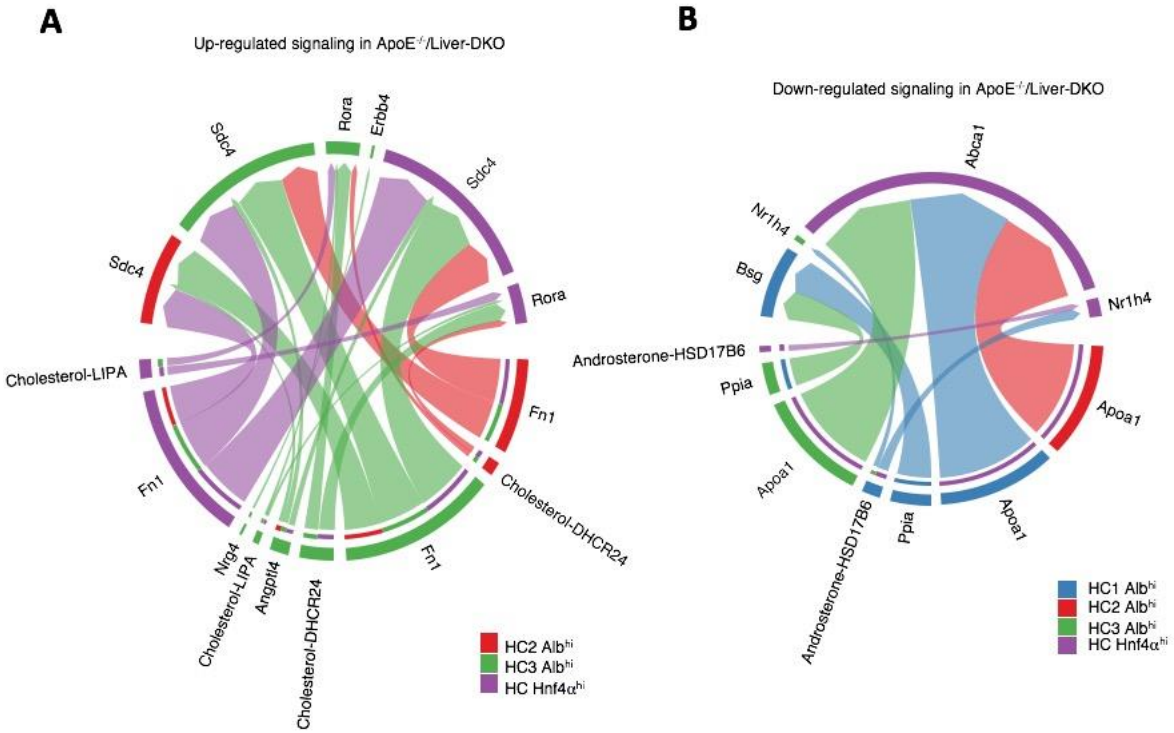

bioRxiv preprint doi: https://doi.org/10.1101/2024.08.26.609742; this version posted August 27, 2024. The copyright holder for this preprint (which was not certified by peer review) is the author/funder, who has granted bioRxiv a license to display the preprint in perpetuity. It is made available under aCC-BY-NC-ND 4.0 International license.

Fig.S10

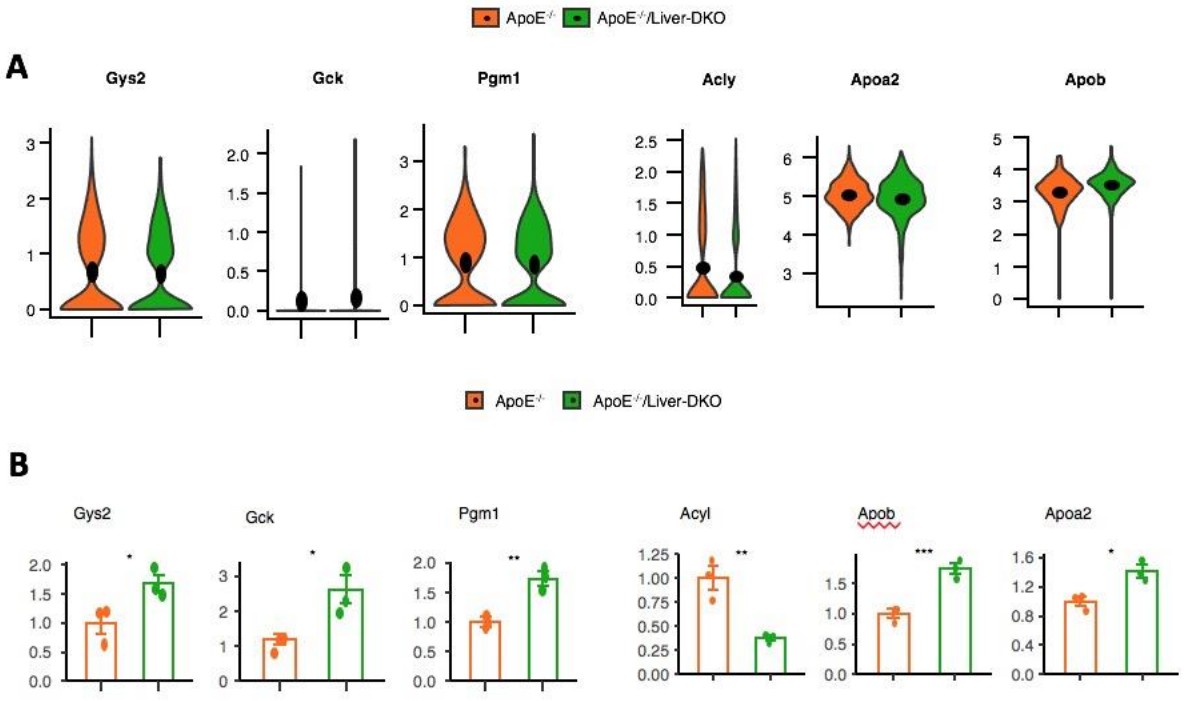

bioRxiv preprint doi: https://doi.org/10.1101/2024.08.26.609742; this version posted August 27, 2024. The copyright holder for this preprint (which was not certified by peer review) is the author/funder, who has granted bioRxiv a license to display the preprint in perpetuity. It is made available under aCC-BY-NC-ND 4.0 International license.

Fig.S11

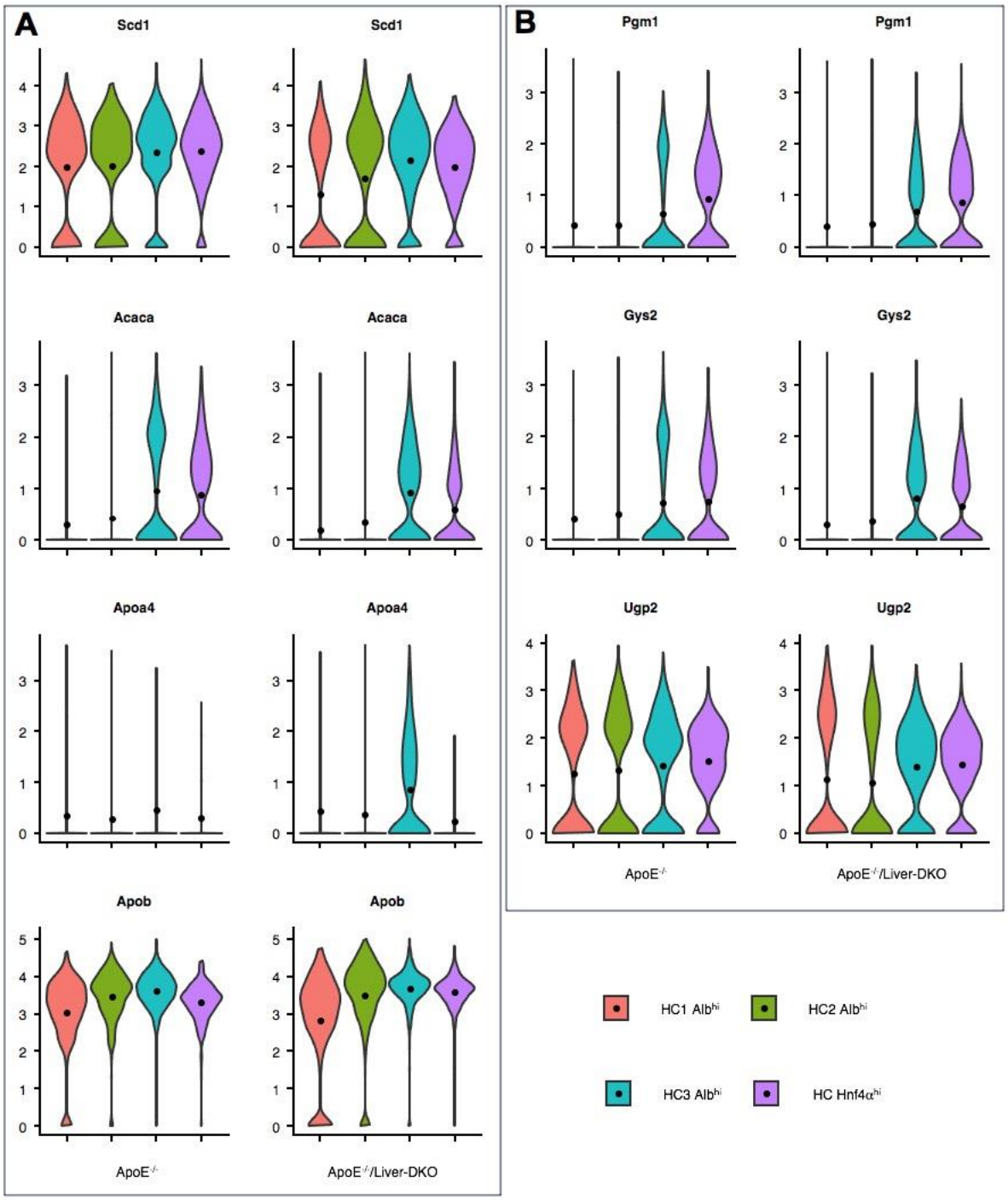

bioRxiv preprint doi: https://doi.org/10.1101/2024.08.26.609742; this version posted August 27, 2024. The copyright holder for this preprint (which was not certified by peer review) is the author/funder, who has granted bioRxiv a license to display the preprint in perpetuity. It is made available under aCC-BY-NC-ND 4.0 International license.

Fig.S12

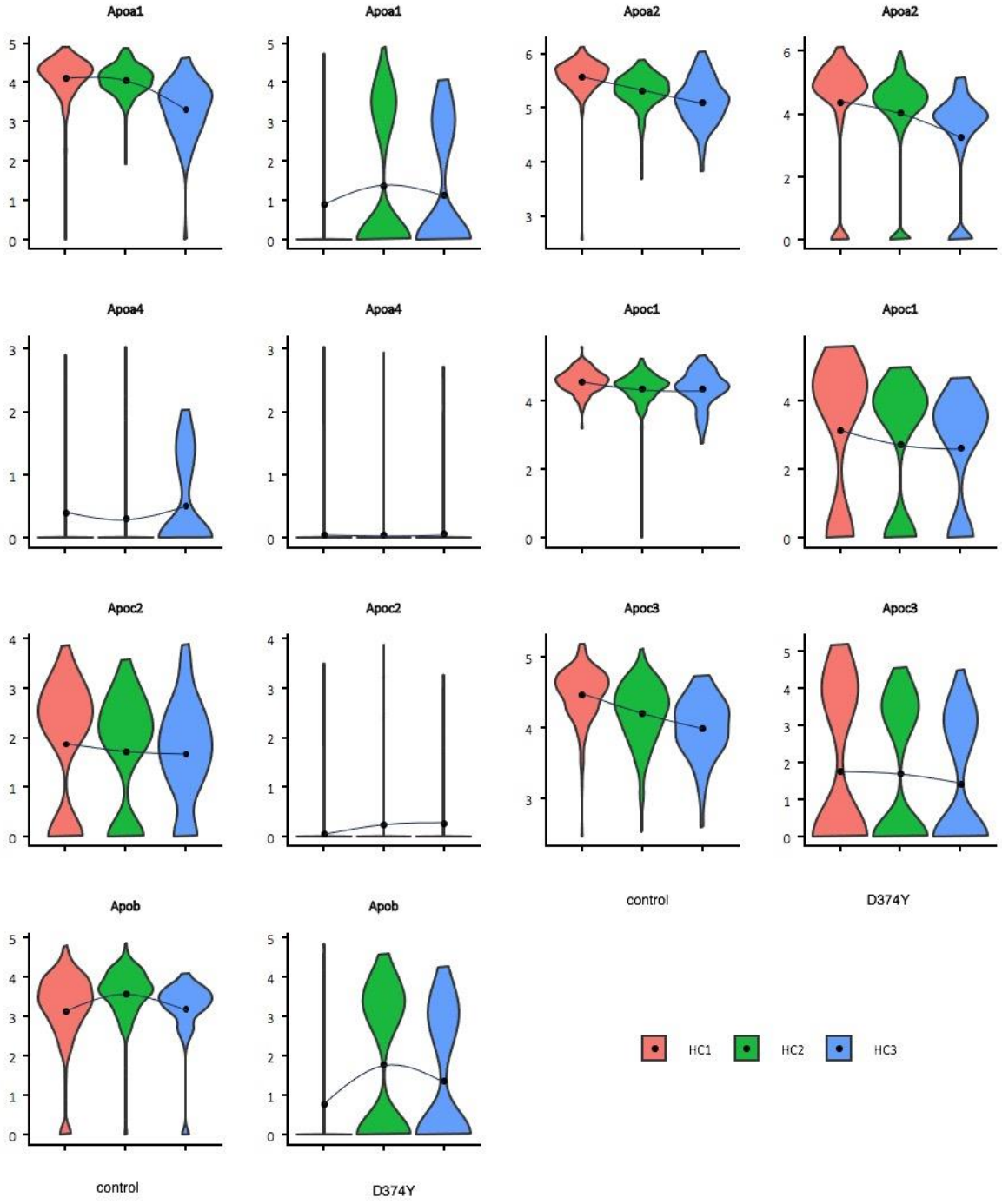

bioRxiv preprint doi: https://doi.org/10.1101/2024.08.26.609742; this version posted August 27, 2024. The copyright holder for this preprint (which was not certified by peer review) is the author/funder, who has granted bioRxiv a license to display the preprint in perpetuity. It is made available under aCC-BY-NC-ND 4.0 International license.

Fig.S13

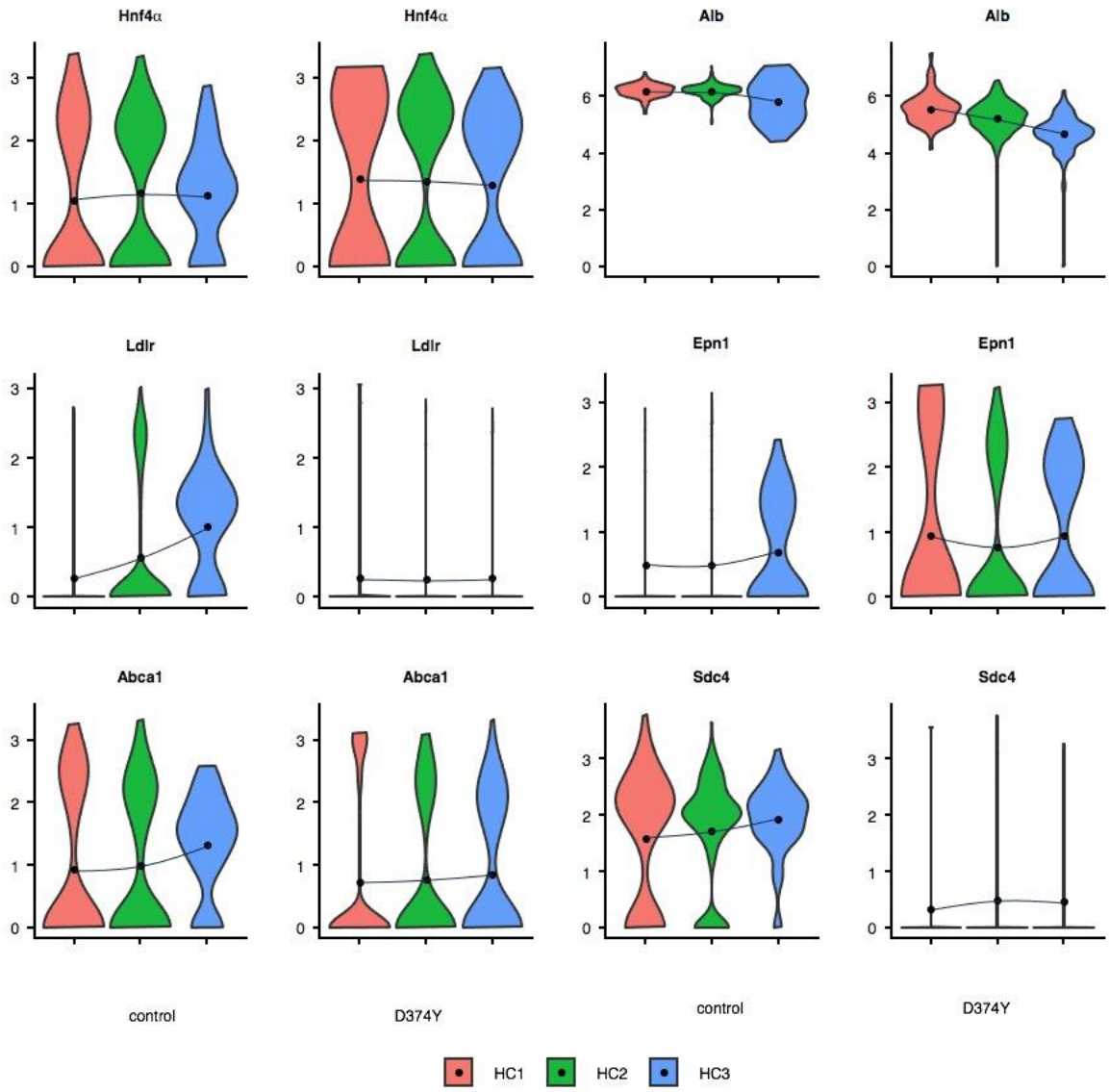

bioRxiv preprint doi: https://doi.org/10.1101/2024.08.26.609742; this version posted August 27, 2024. The copyright holder for this preprint (which was not certified by peer review) is the author/funder, who has granted bioRxiv a license to display the preprint in perpetuity. It is made available under aCC-BY-NC-ND 4.0 International license.

Fig.S14